J Nanostruct 16(2): 4379-4394, Spring 2026

RESEARCH PAPER

Isotherm and Equilibrium Investigation of Methyl Orange Adsorption Using Chitosan-Schiff Base-Cr_2O_3 Nanohybrid

Zainab H. Ghanawi, Zaid H. Mahmoud *

Chemistry Department, College of Sciences, University of Diyala, Iraq

ARTICLE INFO

Article History:
Received 09 January 2026
Accepted 19 March 2026
Published 01 April 2026

Keywords:
Adsorption
Chitosan-Schiff Base-Cr_2O_3
Dye
Nanohybrid
Water treatment

ABSTRACT

A Schiff base-functionalized chitosan/chromium oxide nanocomposite was synthesized and evaluated as an efficient adsorbent for the removal of methyl orange (MO) from aqueous solution. Structural, chemical, and morphological characterization confirmed the successful incorporation of the Schiff base and Cr_2O_3 nanoparticles into the chitosan matrix, resulting in a rough, heterogeneous, and porous surface with abundant active adsorption sites. The fabricated nanohybrid exhibited excellent adsorption performance, achieving approximately 97% MO removal at an optimum adsorbent dosage of 0.05 g under acidic conditions. The adsorption process was strongly influenced by solution pH, with maximum removal observed at pH 3, whereas adsorption efficiency gradually decreased with increasing temperature, indicating an exothermic adsorption process. Equilibrium studies demonstrated that the Freundlich isotherm provided the best fit, while the Langmuir model estimated a maximum adsorption capacity of 80.50 mg g^{-1}. The adsorption mechanism was primarily governed by physisorption through electrostatic attraction, hydrogen bonding, π–π interactions, and surface complexation, demonstrating the nanocomposite's potential for efficient wastewater treatment applications.

How to cite this article
Ghanawi ZH, Mahmoud ZH . Isotherm and Equilibrium Investigation of Methyl Orange Adsorption Using Chitosan-Schiff Base-Cr2O3 Nanohybrid. J Nanostruct, 2026; 16(2):4379-4394. DOI: 10.22052/JNS.2026.02.081

INTRODUCTION

The continuous release of dyes into water systems poses a serious challenge due to their low biodegradability, high chemical stability, and potential toxic effects on both human health and ecosystems. Many dyes have been linked to adverse biological impacts, including allergic reactions, dermatitis, long-term organ toxicity, and carcinogenicity [1-3]. Additionally, effluents containing synthetic dyes can significantly degrade water quality by reducing light penetration, disrupting the balance of dissolved oxygen, impairing photosynthetic activity, and introducing persistent aromatic structures into natural water bodies [4-7]. These toxicological and environmental concerns have made the treatment of dye wastewater a main focus of water treatment research. Many advanced treatments and physicochemical technologies were studied for dye removal, including membrane separation, flocculation, photocatalytic degradation, and adsorption [8-11]. Despite these methods being active under certain conditions, they suffer from severe limitations, including sludge generation, high operating costs, difficult regeneration, incomplete removal, and the potential generation

* *Corresponding Author Email: zaidhameed91@gmail.com*

of harmful secondary by-products [12]. In this context, the adsorption process has emerged as one of the most effective and practical methods, owing to its adaptability, simplicity, ease of operation, and high removal efficiency at high concentrations, without generating toxic conversion products [13-15]. Therefore, developing stable, efficient, and reusable adsorbents remains a key goal in wastewater treatment facilities [16]. Among the different adsorbents reported, chitosan has engaged significant interest as a biodegradable, naturally abundant, biocompatible, and environmentally friendly polymer. Its adsorption behavior is primarily due to the presence of NH2 and OH groups, which can interact via electrostatic attraction, H-bonding, chelation, and surface interactions with different dyes [17]. Because of these groups, chitosan has been largely examined for the uptake of heavy ions, dyes, and other hazardous pollutants. Despite its appealing adsorption chemistry, chitosan suffers from a fundamental limitation that limits its practical applicability, especially in aqueous systems. These restrictions include excessive swelling, poor chemical stability in acidic and basic media, scant mechanical strength, poor dissolution resistance, and comparatively limited surface area. This obstacle often leads to reduced adsorption durability, structural deterioration under working conditions, and reduced regeneration performance, thereby limiting the use of chitosan in realistic water treatment processes [18]. To overcome these limitations, efforts have been focused on the structural and chemical modification of chitosan. Among the available methods, chemical crosslinking is widely recognized as one of the most effective ways to improve the acid resistance, dimensional stability, and mechanical strength of chitosan-based adsorbents. Crosslinking can reduce unnecessary swelling, hinder dissolution, and create a more rigid polymeric structure better suited for repeated adsorption cycles [19]. In this regard, Schiff bases are considered particularly appealing crosslinking agents due to their high reactivity, small molecular size, low cost, and ability to form a close network upon reaction with the NH_2 and OH groups of chitosan [20]. Beyond the simple stabilization of the structure, Schiff base-linked crosslinking may also affect the accessibility and distribution of adsorption sites, hence impacting the balance between adsorption efficiency and mechanical robustness. Improving chitosan performance through an inorganic/organic hybrid has appeared as an active method for enhancing adsorption capacity [21]. Doping oxide nanoparticles into a chitosan matrix can enhance surface heterogeneity, improve chemical and thermal stability, and provide additional active sites for pollutant adsorption. Among these oxides, Cr_2O_3 has been studied extensively due to its chemical stability, surface area, low cost, and toxicity, as well as its broad applicability in functional and environmental materials. However, Cr_2O_3 NPs tend to agglomerate and are difficult to recover after use, which limits their reusability and efficiency. So, introducing Cr_2O_3 into the chitosan matrix provides a practical method to harness the reactivity of the inorganic phase while maintaining the biopolymer's recoverability and functionality [22]. Previous works have shown that composite and crosslinking production can improve adsorption performance. Especially, chitosan/Cr_2O_3 nanocomposites have shown significant potential for H_2O treatment; however, their performance is largely affected by nanoparticle dispersion, crosslinking degree, pollutant characteristics, and surface accessibility [23]. Despite this progress, the mixed impact of Schiff base and Cr_2O_3 doping on the adsorption site and behavior remains insufficiently understood. This restriction is particularly relevant to methyl orange; a permanent anionic azo dye widely used as a model pollutant. In chitosan/Cr_2O_3 nanocomposite systems, methylene orange is expected to occur through H-bonding, interactions with Cr-based surface groups, and electrostatic attraction. However, few studies have investigated how Schiff base crosslinking and Cr_2O_3 incorporation together affect the physicochemical properties and adsorption performance of a single chitosan-based adsorbent. Accordingly, this work aimed to develop a stable crosslinked chitosan-Schiff base/Cr_2O_3 nanocomposite for MO removal from solution, with a focus on material characterization, process optimization, and mechanistic interpretation of adsorption behavior.

MATERIALS AND METHODS

Materials

All chemical materials of analytical grade are employed as received without purification. 4-hydroxybenzaldehyde ($C_7H_6O_2$, 97%), chitosan ((C6H11NO4)n, 85% degree of deacetylation), ethanol (C_2H_5OH, 99.9%), and amine (98%) were

supplied by Sigma-Aldrich. Chromium nitrate ($Cr(NO_3)_3$, 98%) and sodium hydroxide (NaOH, 99%) were procured from Merck Co., while acetic acid (CH_3COOH, 99.5%) and hydrochloric acid (HCl, 35%) were supplied from Loba Chemie.

Synthesis of Schiff base

The Schiff base amino acid was prepared by a condensation reaction between amine and aldehyde. Briefly, 4-aminoacetophenone (2.5 g) was dissolved in 25 mL of absolute ethanol, while 4-hydroxybenzaldehyde (3.3 g) was dissolved in 30 mL of absolute ethanol with 3 drops of acetic acid. Then, the 4-hydroxybenzaldehyde solution was added dropwise to the amine solution with continuous stirring at 30 °C. After that, the mixture was refluxed in a water bath for 6 h, filtered at room temperature, and collected before recrystallization.

Synthesis of Schiff base@chitosan composite

The modification of chitosan was carried out by reacting the amino groups of chitosan with carbonyl-containing aldehyde moieties. Chitosan pellets and 5 g of Schiff base were dispersed in 50 mL of methanol. The mixture was stirred for 3 h at room temperature, yielding pale-yellow pellets. The product was filtered, washed with deionized water and methanol, and dried at 70 °C for 6 h [24].

Synthesis of chromium oxide nanoparticles (Cr_2O_3 NPs)

Cr_2O_3 NPs were synthesized by a solution combustion method employing $Cr(NO_3)_3$ and urea as the oxidizing and fuel precursors, respectively. The reagents were mixed to produce a homogeneous solution, which was then placed in the muffle furnace and heated at 500 °C for 5 h. During heating, the homogeneous solution converted into a gel and ignited via self-combustion. The resulting powder was washed with deionized water and acetone to remove residual impurities and froth, and then dried for 4 h to obtain Cr_2O_3 NPs [25].

Synthesis of Cr_2O_3-Schiff base@chitosan nanocomposite

Surface modification of Cr_2O_3 with Schiff base@chitosan nanocomposite was carried out. Briefly, 1 g of Cr_2O_3 was dispersed in 100 mL of distilled water, after which 1 g of Schiff base@chitosan was dispersed in 100 mL of 1% acetic acid and was added to the chromium solution. The mixture was sonicated at 30 °C for 5 h. The precipitation material was collected, washed with ethanol, and dried at 60 °C for 24 h [26].

Adsorption study

The methyl orange adsorption behavior onto bare chitosan, Cr_2O_3, and Cr_2O_3-Schiff base@chitosan was systematically examined under various conditions. Initial methylene orange concentrations were varied from 10 to 50 mg/L, the pH of the solution was adjusted between 2 and 11 using HCl or NaOH, contact time was varied from 10 to 40 min, adsorbent dosage ranged from 10 to 50 ppm, and temperatures were varied from 25 to 55 °C. After adsorption, the residual methylene orange concentrations were determined via UV-Vis spectroscopy at 420 nm using the Eq. 1:

$$R\% = (Ci - Ce)/Ci * 100\% \quad (1)$$

The adsorption capacity (qe) was calculated using the Eq. 2:

$$qe = (Ci-Ce)*V/m \quad (2)$$

where: Ci and Ce are the initial and equilibrium concentrations of MO, V is the solution volume (L), while m is the adsorbent mass.

RESULTS AND DISCUSSION

Structure characterization

The ^1H NMR spectra of the prepared Schiff bases are shown in Fig. 1. The results show properties consistent with the successful condensation between the amino group of 4-aminoacetophenone and the aldehyde group of 4-hydroxybenzaldehyde. A distinctive signal is observed around 8.4 ppm, which can be attributed to the -CH=N- group. In the region 6.8-8.1 ppm, several signals assigned to the aromatic protons appeared. Moreover, the signals of the ring containing the $-COCH_3$ group appear near 7.8-8.1 ppm, due to the CO group being electron-withdrawing, while the proton signals of the phenol ring appear around 6.8-7.4 ppm, due to the electron-donating effect of the OH group. At 10.0-10.3 ppm, the signal is assigned mainly to the -OH proton, which is credible due to deshielding resulting from conjugation and H-bonding with the aromatic system. On the other hand, the singlet

around 2.5-2.6 ppm is attributed to the 3H of -$COCH_3$. However, the peak at 2.50 ppm overlaps with the DMSO-d6 peak, so the CH_3 signal may be merged with the DMSO signal [27].

The XRD of the prepared Cr_2O_3 is shown in Fig. 2. The results confirm the formation of the α-phase of a rhombohedral crystal structure with main diffraction peaks located at 24.45°, 33.61°, 36.17°, 41.50°, 44.14°, 50.10°, 54.86°, 63.33°, 65.14°, 74.05°, 76.86°, and 79.06° are corresponding to (012), (104), (110), (133), (202), (024), (116), (214), (300), (1010), (220) and (223) which assign to α-Cr_2O_3 and two diffraction peaks centered at 39.69° and 58.37° back to Cr_3O_4. Furthermore, the results indicate that the (104) diffraction peak is most intense, suggesting that this crystal plane is the most discriminatory growth orientation. On the other hand, the narrow and sharp peaks suggest good structural ordering and high crystallinity. The blue star-marked diffraction peaks indicate the existence of a minor Cr_3O_4 phase, indicating that the formation is predominantly Cr_2O_3 with a small

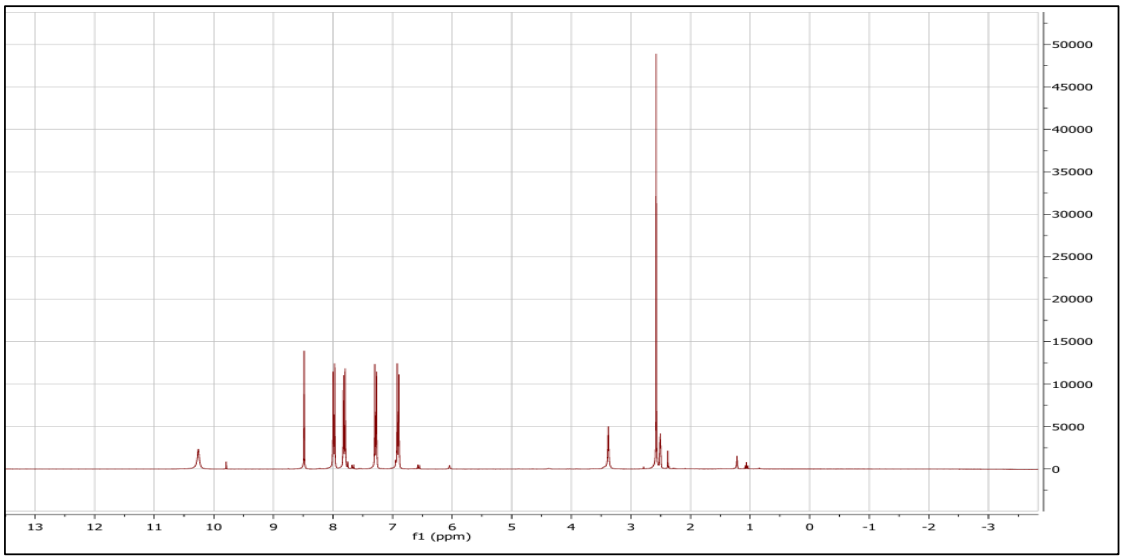

Fig. 1. ^{1}H NMR spectra of the prepared Schiff base.

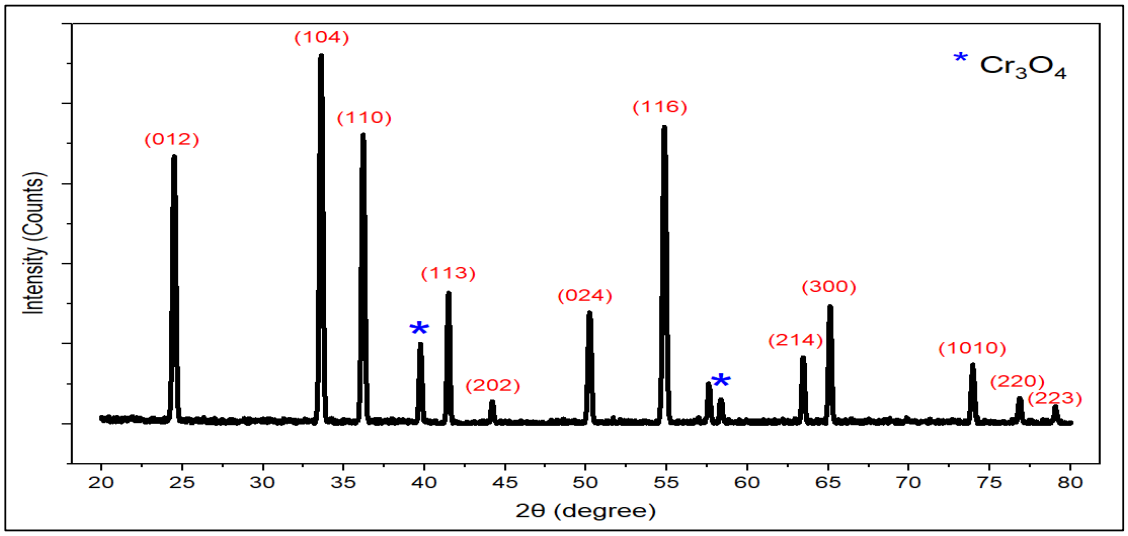

Fig. 2. XRD of Cr_2O_3 nanoparticles.

quantity of Cr_3O_4 [28].

The XRD of chitosan is shown in Fig. 3. The spectrum appears to have two broad diffraction peaks centered at 9.96° and 19.98°, corresponding to the (020) and (200) planes. These diffraction peaks are distinctive of the semi-crystalline structure of chitosan. The broad diffraction peak at 9.96° is assigned to the ordered arrangement of chains and hydrated crystalline regions. In contrast, the stronger diffraction peak is related to intramolecular and intermolecular H-bonding between the glycosidic, hydroxyl, and amino groups in the chitosan structure. The broad diffraction peaks suggest that the chitosan is not highly crystalline, but has both amorphous and crystalline regions. Furthermore, the absence of other diffraction peaks indicates high purity [29]. For Chit-Schiff base, the results showed that the two diffraction peaks of chitosan (020) and (200) were still observed after incorporation of the Schiff base, indicating preservation of the chitosan backbone. However, the intensity, width, and position of the (200) peak varied notably, suggesting that incorporating S compounds strongly affects the arrangement of chitosan chains. After adding the Schiff base, the NH_2 groups of chitosan reacted with CHO to produce -C=N- . As a result, in chitosan, the H-bonding network is partially dissociated and replaced by C=N-related interactions, pi-pi interactions, H-bonding, and dipole-dipole interactions, depending on the S structure. For incorporated Cr_2O_3, the results illustrated the successful production of nanocomposites. In all prepared compounds, the diffraction peaks associated with chitosan are still observed, corresponding to the semi-crystalline structure of chitosan. The conservation of these broad diffraction peaks suggests that the chitosan structure was preserved after Schiff base and metal oxides incorporation. For the chitosan-Schiff -Cr_2O_3 nanocomposite, eight diffraction peaks are shown and correspond to Cr_2O_3, containing reflections associated with the (104), (110), (113), (024), (116), (214), (300), and (1010) crystal planes. Compared with bare chitosan, the Cr_2O_3 diffraction peaks are of comparatively low intensity, indicating better dispersion and smaller crystallites. The remaining Schiff base region suggests that the Schiff base still participates significantly in the composite structure. In addition, the results appear to show changes in width, intensity, and shape of the (200) diffraction peak after incorporation of metal oxides. These alterations indicate that interactions between functional groups of chitosan-Schiff base and metal oxides affect chain packing and chitosan-Schiff matrix crystallinity. The overlap between the oxides and chitosan diffraction peaks suggests interfacial interactions between the inorganic and organic phases [30].

Fig. 4A-D shows the FESEM images of the

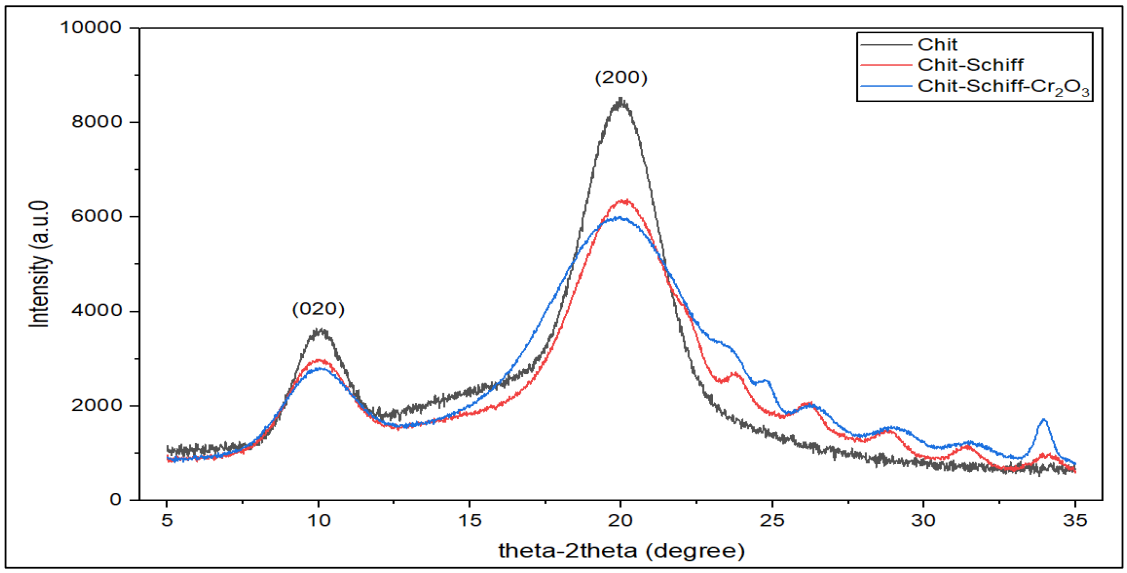

Fig. 3. XRD of chitosan, chitosan/Schiff base and chitosan/Schiff base-Cr_2O_3.

prepared compounds. The results exhibit clear variation in surface morphology, suggesting that the structure of the Schiff-base compound strongly impacts aggregation behavior, particle growth, and surface organization. The Schiff-base compound (Fig. 4A) demonstrates an irregular flake morphology consisting of stacked plates. Furthermore, it exhibits a highly aggregated and rough state, which may be assigned to dipole-dipole, H-bonding, and pi-pi bonding forces between Schiff-base units. The morphology indicates the production of closely packed regions with finite-separation domains. For Cr_2O_3 (Fig. 4B), the results showed that the surface consists of agglomerated NPs coordinated in cauliflower morphology. The particles are obtained as tiny circular grains that are connected to produce a close agglomerate with a tough surface structure. This morphology indicates fast nucleation pursued via agglomeration, which generally results from the high surface-area energy of freshly produced NPs. The tough, agglomerated structure can supply numerous surface-active sites, making it appropriate for adsorption applications. For Schiff-

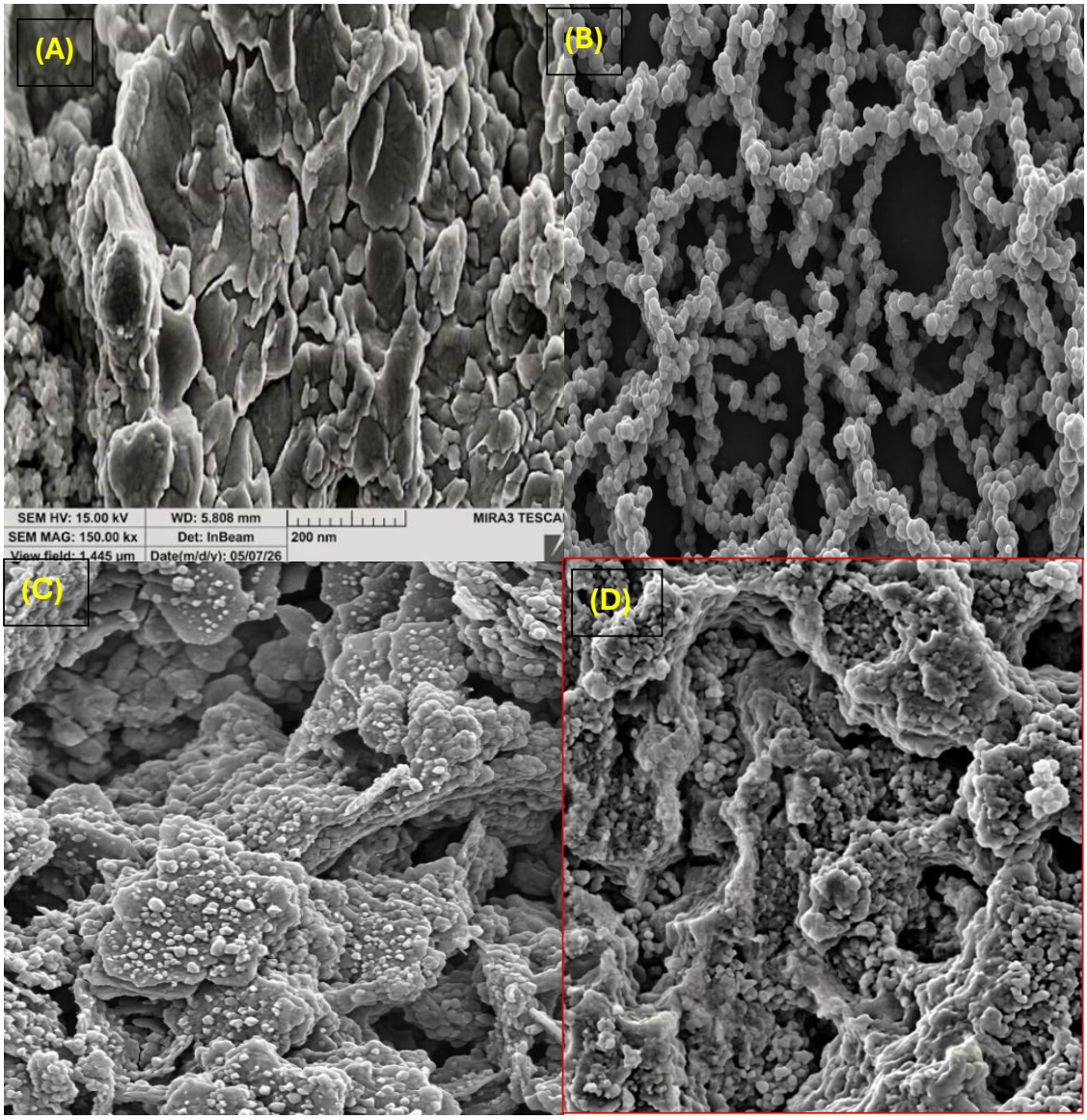

Fig. 4. FESEM of (A) Schiff-base, (B) Cr_2O_3, (C) chitosan/Schiff base and chitosan/Schiff base-Cr_2O_3.

base/chitosan (Fig. 4C), the results reveal that the original chitosan network is less clearly defined and is substituted by irregular, closely spaced areas with granular and plate surface properties. Various small particles are spread on the chitosan sheets, resulting in a clearly tougher and more heterogeneous surface. This morphological conversion indicates that the Schiff-base units are deposited over the matrix, thereby changing the native chain arrangement. The production of tough granular areas is proportional to improved intermolecular interactions containing the aromatic segments, -C=N- groups, and chitosan chains. For the Schiff base/chitosan-Cr_2O_3 nanocomposite (Fig. 4D), the results indicate a denser and more granular structure. Furthermore, it appears that there are a higher surface coverage degree and stronger agglomeration. In addition, the Cr_2O_3 NPs spread across the external surface and within the pores, partially filling the porous spaces. This suggests that Cr_2O_3 NPs may have a greater tendency toward agglomeration and nucleation on the Schiff base/chitosan surface. The intensive granular morphology indicates stronger interaction between the functional groups of Schiff base/chitosan and Cr_2O_3 nanoparticles [31-34].

Adsorption performance

Optimization parameters

As can be seen from (Fig. 5A), the adsorption percentage of the dye (methyl orange) is found to be higher as the adsorption time is longer for all the adsorption surfaces studied. The adsorption process was very fast, particularly in the first stage, the first 30 minutes, as a result of the number of active sites on the surface of the adsorbents. The surface hydroxyl groups of these sites can interact with the molecule of methyl orange via hydrogen bonding, electrostatic interactions, surface coordination, and π–π interactions. After this very fast period, the amount of adsorption decreased and levelled off between 90 and 120 minutes. The dye reduction adsorbed could be attributed to the continual saturation of the active sites with dye and to the decrease in the concentration of dye in the solution as the dye is being drawn towards the surface of the adsorbent. The performance of the adsorption efficiency for Chit–Cr_2O_3/Schiff base > Chit > Cr_2O_3. The lowest adsorption efficiency of chitosan is explained by the less protonation of the amino groups of chitosan at neutral pH as compared to the other pH values, thus decreasing the electrostatic attraction between the anionic dye (methyl orange) and chitosan. At the same time, adsorption of chromium oxide was slightly higher than chitosan because of the presence of the Cr–OH groups and the metal oxide surface sites, which can bind the dye. However, the addition of Cr_2O_3 to chitosan added a lot of improvement, suggesting that it has a synergistic effect when combined with chitosan. The presence of amino group, hydroxyl groups in chitosan and hydroxyl groups and more metal active centers in chromium oxide. This is further modification of the Chit–Cr_2O_3 composite material with Schiff bases, which further enhanced the adsorption performance. This is mainly because of the presence of other functional groups like azomethine C=N, phenolic OH, carbonyl C=O and aromatic rings. As the number of adsorption sites increases, the number of interactions between molecules of methyl orange increases; hence, these groups are more interactive with the active groups. The π–π interactions of the aromatic structure of the Schiff bases could also be responsible for their involvement in the aromatic system of the methyl orange [35]. The influence of pH on the adsorption of methyl orange is evident from (Fig. 5B) which shows that the rate of removal of the dye is strongly dependent on the acidity or basicity of the medium. The results indicated that the best percentage of removal was achieved at pH 3 and the percentage of removal decreased with increasing pH (5, 7, 9 and 11) for all the adsorbents used. The behavior can be scientifically explained as it is an anionic dye containing mainly $–SO_3^-$ group which will have a stronger affinity towards the positive charge on the surface of the adsorbent in acidic condition. In the reaction given below the amino groups of chitosan gets protonated, thereby making the surface of the adsorbent positively charged and the electrostatic force of attraction between the adsorbent and the negative charge of the molecule of Methyl orange increases: $–NH_2 + H^+ \rightarrow –NH_3^+$ Moreover, surface hydroxyl groups of chromium oxide can be protonated under acidic conditions to form a positive surface site e.g. $Cr–OH_2^+$. Thus, in an acidic environment, chitosan is able to enhance the interaction between dye and surface and the adsorption efficiency is maximum for chitosan and chromium oxide. If the pH is greater than 5 the degree of surface protonation will be less, but not significantly less than the pH 3, and the pH will not

be as effective as the pH 3 in removing the contaminant. The moderate adsorption observed from the previous result (neutral contact time) is displayed in the following result. Also, the protonation of the amino group of chitosan is small, as is the electrostatic attraction between the surface of chitosan and the methyl orange. Hence, non-electrostatic forces like hydrogen bonding, π–π interaction, surface complexation and hydroxyl, carbonyl or azomethine groups are more significant for the adsorption at pH 7. In the alkaline condition the pH is 9 and 11, the

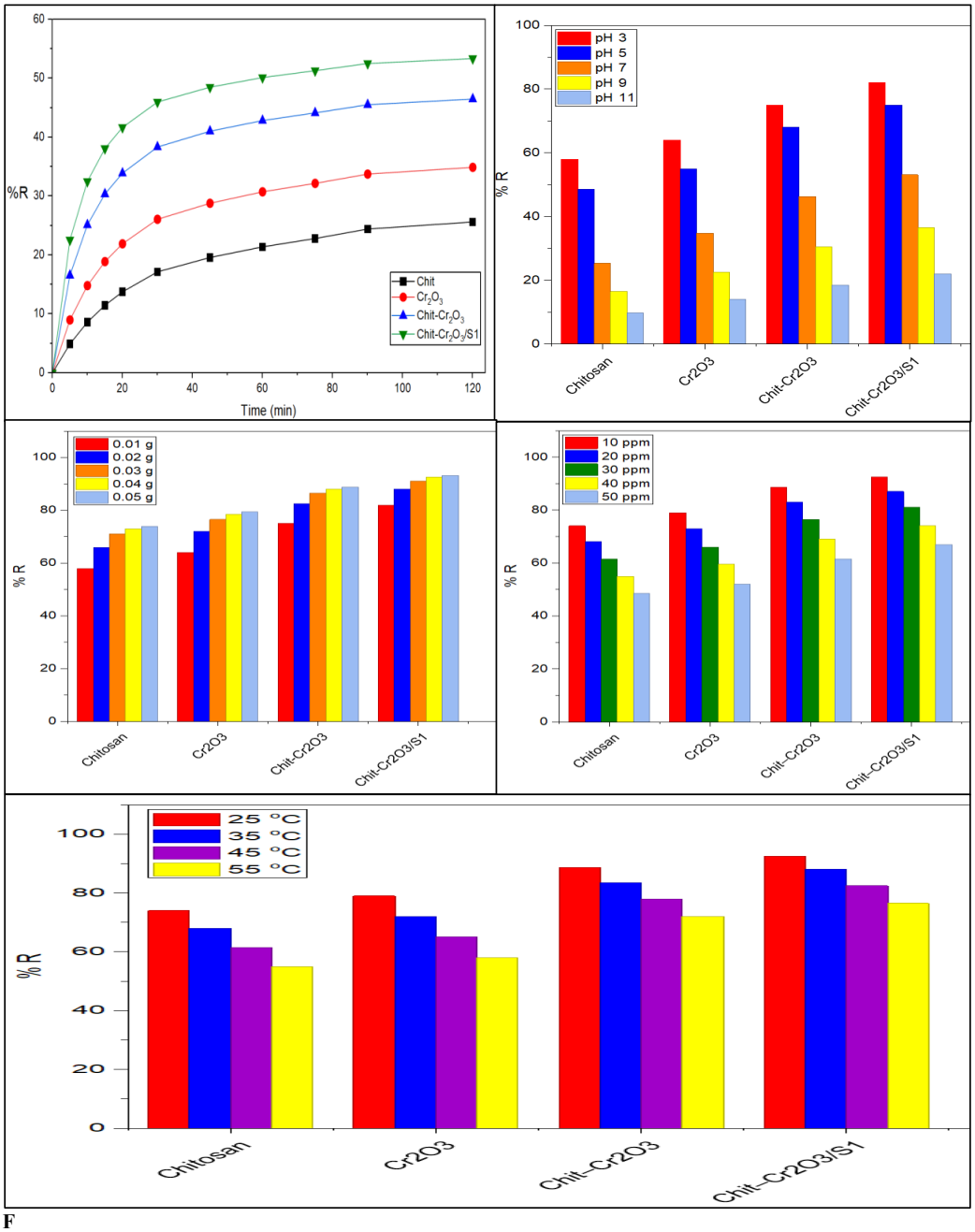

F

Fig. 5. Effect of (A) contact time, (B) pH, (C) dosage adsorbent, (D) dosage of dye, (E) temperature for adsorbing MO on prepared nanocomposites.

adsorption efficiency is greatly reduced. This is because aminos and hydroxyls can be deprotonated on the surface of the adsorbent, thus decreasing the positive surface charge, and possibly increasing the negative surface charge. Besides, the concentration of OH^- ions are high in alkaline solution and this will compete with the concentration of OH^- ions available in the adsorption sites in the presence of methyl orange. This leads to a lesser interaction of the adsorbent surface with dye which decreases the percentage of dye removal. The removal efficiency was the least for chitosan as it had the most dominant adsorption property of amino and hydroxyl groups, which is less effective at neutral and alkaline conditions. The surface hydroxyl groups and active sites of chromium oxide are shown to be beneficial for its performance than chitosan. The adsorption efficiency was noted the combination of chitosan and chromium oxide (Cr_2O_3) in a synergistic manner. The modification of surface by a Schiff base yielded the best adsorption efficiency composites. This is because it contains other active functional groups (C=N, OH, C=O and aromatic rings). These groups create more adsorption sites, and by forming various interactions with the molecule of the methyl orange, such as hydrogen bonding, π–π interactions, polar and surface complexation. The highest results were given by Chit–Cr_2O_3/Schiff base which may be attributed to the greater percentage of the effective binding groups (phenolic hydroxyl groups) available to interact with the methyl orange in the entire pH range [36,37]. The effect of adsorbent dose on removal efficiency of the methyl orange under optimized condition, is shown in Fig. 5C, where the dose of adsorbent has been varied between 0.01 g and 0.05 g. The overall percentage removal was found to be a function of the dosage of all the adsorbents used on all surfaces investigated. This effect is attributed mainly to the increase in the active adsorption sites that results with the increase of mass of the adsorbent. The more the other functional groups such as –OH, $–NH_2$, C=N, C=O and Cr–OH groups which can interact with the molecule of methyl orange, the higher the dose. The removal efficiency of chitosan went up from about 58% to around 74% with increase in the amount of chitosan used from 0.01 g to 0.05 g. Chitosan has amino and hydroxyl functional groups and the removal efficiency, the lowest among all other adsorbents studied, was found to depend on the amount of these functional groups of the polymer. The compound's higher performance compared with chitosan (from about 64% to almost 79%) could be due to the hydroxyl groups present in the surface of the compound and the presence of metal-oxide active sites. The composite of Chit–Cr_2O3 improved significantly as compared to chitosan and Cr_2O3 in which Cr_2O3 removal increased from ~75% to ~89%, respectively. This is another proof of the synergic effect of the surface of the inorganic chromium oxide and the organic matrix chitosan. The results indicated that the main reasons for the better adsorption of MO on the chitosan/Cr_2O_3 composite were the amino and hydroxyl groups of the chitosan molecule, and the hydroxyl groups and metal-active centers of the Cr_2O_3. The highest removal efficiencies in all the range of dosage were achieved with the use of the modified composites by Schiff base. The introduction of additional functional groups like the azomethine C=N, the phenolic OH, the carbonyl C=O and aromatic rings due to the presence of Schiff base structures has been proposed as the source of this improvement. The presence of these groups (which can hydrogen bond, electrostatically attract and interact with π-electrons and even surface complex with the molecules of methyl orange) can facilitate the adsorption process. In this regard, Chit–Cr_2O_3/Schiff base exhibited the maximum removal efficiency at 0.05 g with almost 97% dye removal efficiency as it may possess a greater number of active binding sites with more interaction with dye molecules. Moreover, it is observed that the removal efficiency does not improve significantly with the increase of dose, particularly in the dose range 0.04–0.05 g. This means that the adsorption is very close to the limiting value of adsorption which corresponds to a further increase in the amount of adsorbent added it would result in very little increase in adsorption. Therefore, it is concluded that a removal percentage of 0.05g is the optimum one but 0.04g gives almost the same removal percentage with a lesser amount of adsorbent [38,39]. In the case of the dye used, the efficiency of removal was found to be lower with higher initial dye concentration (10 to 50 ppm) for methyl orange (MO) (Fig. 5D). This is because there are only a few adsorptive sites at the surface of the adsorbent. At these sites with low dye concentration, these sites are adequate to bind

most of the dye molecules and so a high percentage of dye is removed. But at higher concentrations, the number of molecules of methyl orange will be greater to compete for the limited number of sites and the efficiency of removal will be less since the surface would be saturated. The dye binding was enhanced compared to hydrogen bonding, electrostatic attraction, π–π interaction and surface complexation due to the increased number of active groups present in the Schiff base modified composites which includes C=O, OH, C=N, aromatic rings etc. In these, the maximum efficiency was found with Chit–Cr_2O_3/Schiff base, where a higher number of efficient adsorption sites was available. As the concentration of the dye increases, the removal percentage was observed to decrease; however, the adsorption capacity is expected to increase since more dye molecules is more to be loaded onto the surface of the adsorbent [40]. Methylene orange adsorption on the prepared adsorbent was affected by the prepared adsorbent, as depicted in Fig. 5E, which shows the effect of temperature. The sorption of methyl orange showed a slight decrease with increasing temperature from 25 to 55 °C, indicating that the sorption process was mostly exothermic. The molecules of methyl orange are more strongly adsorbed on the surface of the adsorbent in the cold state, and hence it is more efficient. The interactions can be electrostatic attraction, hydrogen bonding, π–π interaction, and surface complexation. The molecules of the dye have more energy at higher temperatures. This results in the formation of less stable molecules of methyl orange, which are absorbed onto the surface, and some molecules desorb. Furthermore, there is a possibility that the interaction between the molecules of dye and the adsorbent surface will be reduced as the temperature is increased. Thus, the removal efficiencies are lower at 35 °C, 45 °C and 55 ° C than that at 25 ° C. The removal efficiency of the Schiff base modified composites was found to be higher as some of the active functional groups (azomethine C=N, hydroxyl OH, carbonyl C=O and aromatic rings) were present in the modified composites. The number of adsorption sites increases and more interactions with the molecules of methyl orange are enhanced in these groups. This gave the best results for the composition Chit–Cr_2O_3/Schiff base, which can be correlated with the number of effective binding sites [41].

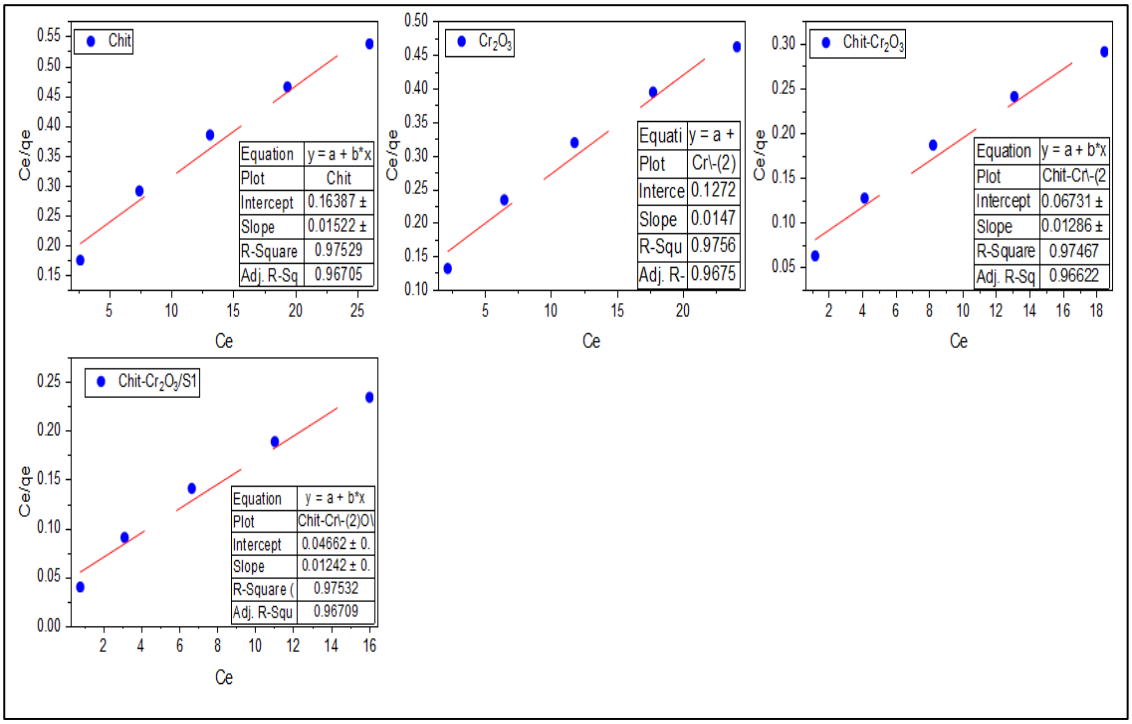

Fig. 6. Langmuir isotherm for adsorbing MO on prepared materials.

Isotherm study

The adsorption isotherms were obtained and the behavior of the isotherm was studied by various MO dye and prepared adsorbents, such as Langmuir, Freundlich and Temkin and Dubinin–Radushkevich adsorption isotherms. The Langmuir plots (Fig. 6) demonstrate that there is a high linear correlation coefficient for all the adsorbents tested with a relatively high R^2 value that is around 0.97. The adsorption of dye (methyl orange) perfectly obeyed the Langmuir adsorption isotherm, which suggests the dye is adsorbed in a monolayer on the surface of the available adsorption active sites of the adsorbents.

The Langmuir fitting is represented by:

$$Ce/qe = 1/(q_{max} K_L) + Ce/q_{max} \quad (3)$$

Where qmax is the maximum flow, K is the degradation rate and L is the biomass at the start of the simulated time. By observing the plots, it could be noticed that the slope which is determined by the slope of the graph, decreased with the increase in the amount of chitosan modified to Chit–Cr_2O_3/Schiff base after the modification, thereby increasing the adsorption capacity (qmax). This will give rise to an enhancement in the surface adsorption capacity upon incorporation of Cr_2O_3 and Schiff base groups. Compared with the other polymers, the Langmuir capacity of chitosan is the lowest because of its number of available active adsorption sites, which are mainly –OH and $–NH_2$ groups, are few. The surface-active sites of the metal oxides in Cr_2O_3 and Cr – OH groups in Cr_2O_3 are helpful to improve the adsorption capability. The surface centers of chromium oxide and the functional groups of chitosan are present in the composite material (Chit–Cr_2O_3) which is the reason for the high capacity of the composite material and its better fitting. The other groups present in the Schiff base modified composites (C=N, OH, C=O and aromatic ring) exhibited the best Langmuir behavior. These groups can provide additional binding sites, and increase the interaction with the methyl orange via hydrogen bonding, electrostatic attraction, π–π interaction and potential surface complexation [42].

As shown in Freundlich isotherm plots (Fig. 7) all the used adsorbents have good linear relationship between adsorption capacity (log qe) and equilibrium concentration (log Ce) for the adsorption of methyl orange. The results of the adsorption data have been well correlated with Freundlich model and the value of R^2 ranges from 0.991-0.994. This implies that the adsorption energy of the adsorption sites on a heterogeneous surface is not the same and the molecules of methyl orange can be adsorbed. The Freundlich

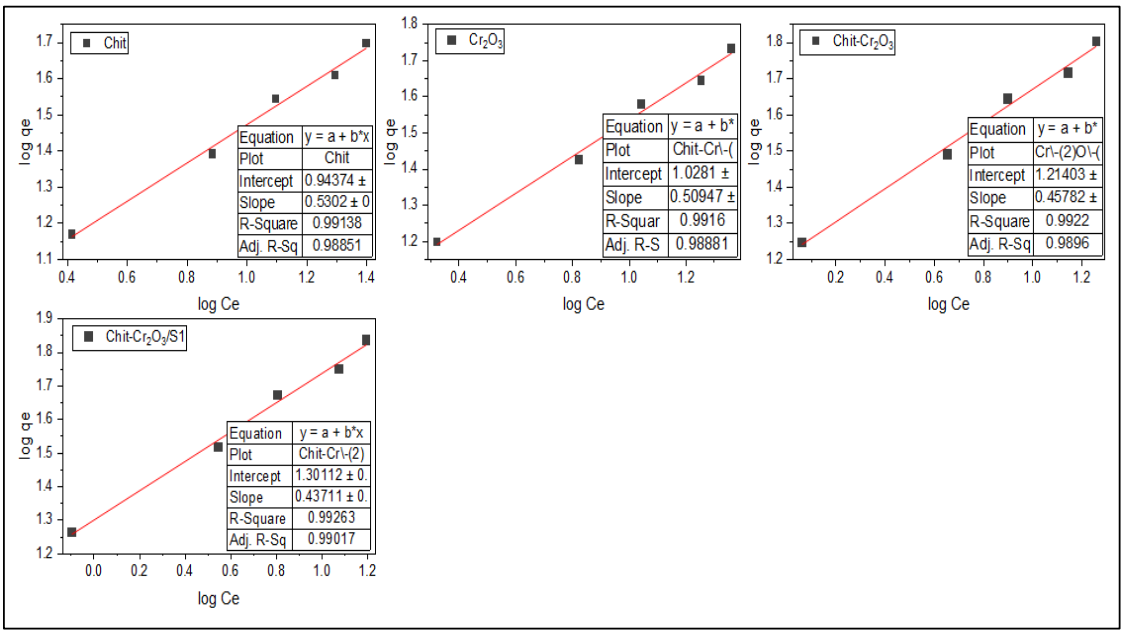

Fig. 7. Freundlich isotherm for adsorbing MO on prepared materials.

model is given by:

$$\log qe = \log KF + (1/n) \log Ce \quad (4)$$

In Plots are linear and the slope is equal to 1/n and the intercept is equal to log KF. The values of 1/n obtained are < 1 for all the adsorbents, this indicates that the adsorption process is favorable. This also shows that as the binding strength increases, the concentration of the molecule of the dye also increases at different binding sites as expected in a composite material functionalized with chitosan, chromium oxide and Schiff base. However, the Freundlich constant (KF) was

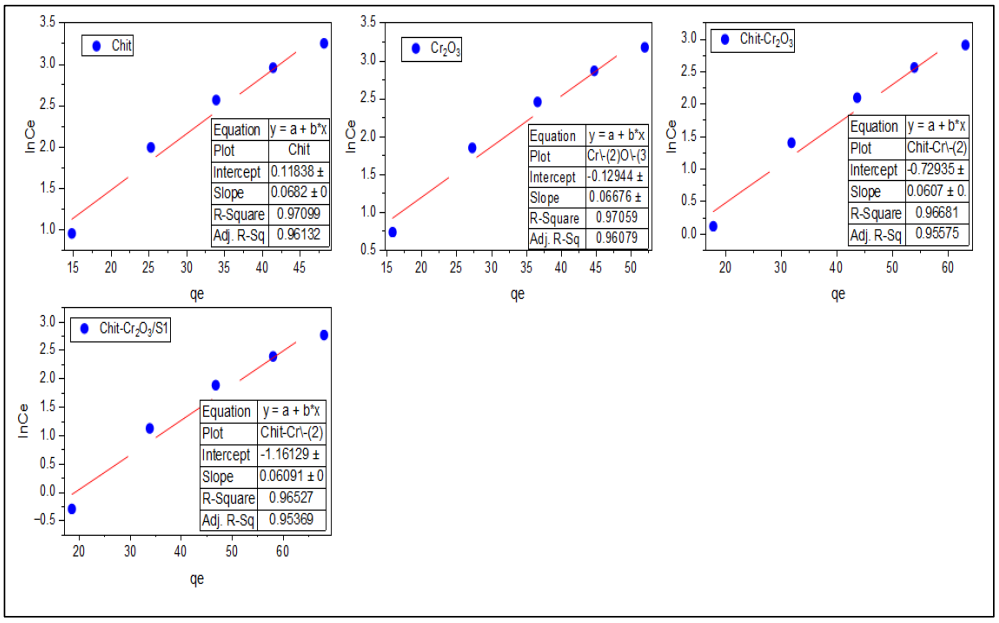

Fig. 8. Temkin isotherm for adsorbing MO on prepared materials.

Table 1. Adsorption isotherm parameters for methyl orange on the prepared adsorbents using the Langmuir, Freundlich, Temkin, and Dubinin–Radushkevich models.

	Langmuir		Freundlich	
Adsorbents	qmax	KL	KF	n
Chitosan	65.7007	0.0929	8.7850	1.8861
Cr_2O_3	67.9510	0.1156	10.6685	1.9628
Chit–Cr_2O_3	77.7654	0.1911	16.3692	2.1843
Chit–Cr_2O_3/Schiff	80.4887	0.2665	20.0043	2.2877
	Temkin		D-R	
	B	KT	qm	β	E
Chitosan	14.2373	0.9495	38.7896	1.5440	0.5691
Cr_2O_3	14.5376	1.2222	41.5166	1.0780	0.6811
Chit–Cr_2O_3	15.9277	2.2636	49.2557	0.4285	1.0803
Chit–Cr_2O_3/Shiff	15.8486	3.5252	52.5293	0.2445	1.4299

increased along with the modification of chitosan by Chit–Cr_2O_3/Schiff base indicating that the modified chitosan has good adsorption property. The additional active groups present in the molecules are –OH, –NH_2, C=N, C=O and Cr–OH and presence of aromatic rings in the structure of Schiff base are responsible for this improvement. These groups enhance the number of adsorption sites and are able to interact with methyl orange by hydrogen bonding, electrostatic force and π–π interactions and surface interactions. The Chit–Cr_2O_3/Schiff base as the best adsorbent, showing good Freundlich behavior of the adsorbent, which is indicated by the best adsorption capacity and best Freundlich model fit with all the adsorbents. The result obtained above indicates that surface-modified S4 has the best adsorption property, as shown by the above result on the adsorption of methyl orange. High R^2 values for the overall also indicate that the Freundlich model applies to this adsorption system while the models that assume the surface of the adsorption system is truly homogeneous do not apply [43].

As shown in the plots (Fig. 8), a good linear relationship was obtained between the values of lnCe and qe with relatively high R^2 values (0.95-0.97) for all the adsorbents studied showing the adsorption of methyl orange. This implies that the Temkin model can be used for adsorption process. Good fit implies that in addition to availability of active sites, the interaction between adsorbent-adsorbate and/or perhaps between adsorbed dye molecules on the surface is also a factor in adsorption. Based on the Temkin model (Table 1) it is believed that the heat of adsorption during the process of adsorption is not constant but is gradually decreasing as the surface is covered by the molecules of methyl orange. This is a natural phenomenon as in the initial adsorption process most of the active sites are available which in turn can be adsorbed by the dye molecule. Once filled in these sites will be filled at the less binding energy sites, the energy will decrease from site to site. The adsorption property of the modified composites was improved as compared to that of chitosan and Cr_2O_3. This is attributed

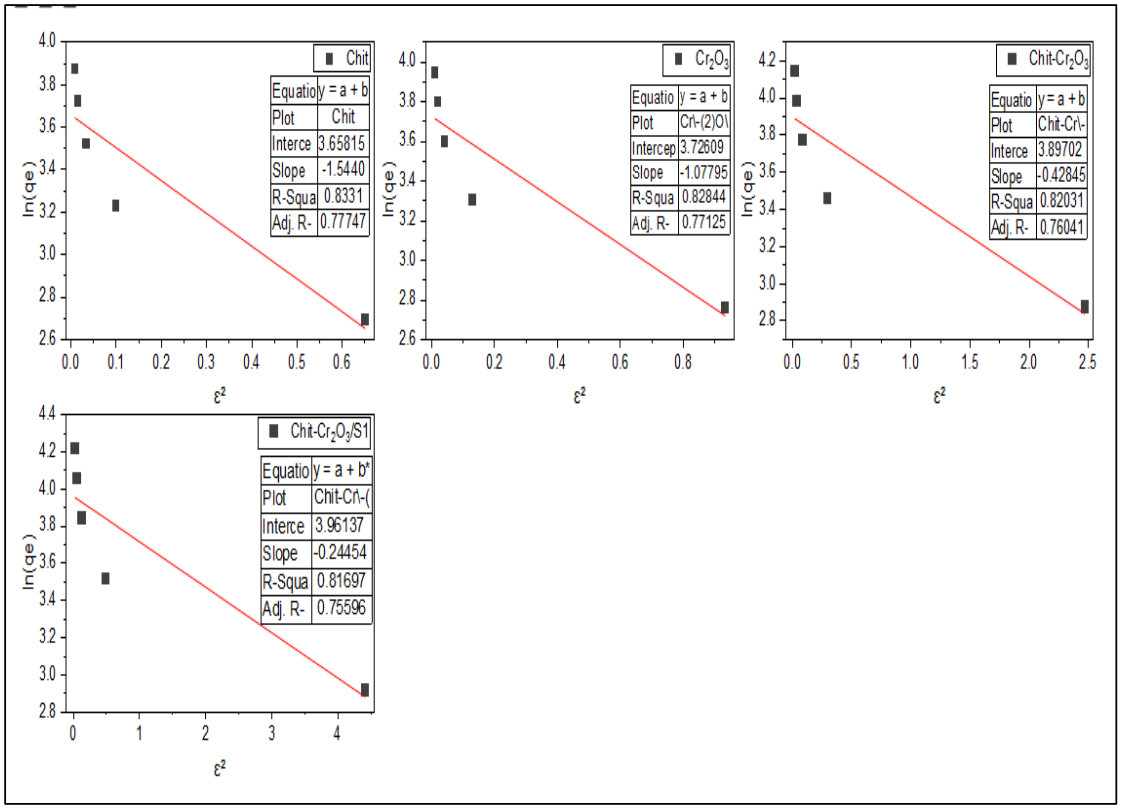

Fig. 9. Dubinin–Radushkevich isotherm for adsorbing MO on prepared materials.

to other functional groups which are present in the modified materials such as C=N, OH, C=O and aromatic rings. These would increase the number of active sites, increase the hydrogen bonding, electrostatic attraction/ π–π interactions between the methyl orange and surface, and increase the surface complexation [44].

The Dubinin–Radushkevich (D–R) isotherm plots of ln (qe) versus ε^2 for adsorption of methyl orange on the prepared adsorbents are presented in Fig. 9. The plots are moderate linear which is around 0.81-0.83, which shows that the D–R model can explain the nature of adsorption but is not the best model to describe the adsorption equilibrium as compared to the Langmuir model or the Freundlich model. The negative slope shown in all plots is consistent with the linear form of the D–R equation:

$$\ln qe = \ln qm - \beta\varepsilon^2 \quad (5)$$

The adsorption capacity decreases with this behavior as the Polanyi potential. The mean adsorption energy E can be calculated by using the D–R model. As the heat of adsorption is less than 8kJ/mol this shows that adsorption is predominantly physical adsorption. This is because the interactions between the molecule and the molecules of the adsorbent are weak to moderate: (Hydrogen bonding, electrostatic attraction, π – π interaction and surface interaction between the molecule and the adsorbent). This indicates that the adsorption capacity of the modified sample has increased, which is attributed to the extra functional groups –OH, $–NH_2$, C=O, C=N and Cr–OH groups of the modified sample. Based on the overall conclusion, it can be stated that the adsorption process that occurs is primarily physical, as the R^2 value is small, meaning that the D–R model is not as suitable as the Freundlich and Langmuir models, and can describe the behavior of the adsorption process in equilibrium [45].

CONCLUSION

Schiff base-incorporated chitosan/Cr_2O_3 nanocomposite was successfully synthesized and displayed a heterogeneous, granular surface with abundant adsorption-active sites. The nanocomposite appeared the highest MO removal efficiency among the estimated materials, reaching approximately 97% at an adsorbent dosage of 0.05 g, although 0.04 g produced a comparable result with lower material consumption. Adsorption was favored under acidic conditions, particularly at pH 3, and reduced with increasing temperature from 25 to 55 °C, suggesting the exothermic nature of the process. The equilibrium data were best described via the Freundlich model, suggesting favorable adsorption on an energetically heterogeneous surface, while the maximum Langmuir adsorption capacity of the nanocomposite reached 80.50 mg/g.

CONFLICT OF INTEREST

The authors declare that there is no conflict of interests regarding the publication of this manuscript.

REFERENCES

1. Hsu C-Y, Ajaj Y, Mahmoud ZH, Kamil Ghadir G, Khalid Alani Z, Hussein MM, et al. Adsorption of heavy metal ions use chitosan/graphene nanocomposites: A review study. Results in Chemistry. 2024;7:101332.
2. Abdul-Reda Hussein U, Mahmoud ZH, Alaziz KMA, Alid ML, Yasin Y, Ali FK, et al. Antimicrobial finishing of textiles using nanomaterials. Braz J Biol. 2024;84.
3. Mahmoud ZH, Al-Bayati RA, Khadom AA. The efficacy of samarium loaded titanium dioxide (Sm:TiO_2) for enhanced photocatalytic removal of rhodamine B dye in natural sunlight exposure. J Mol Struct. 2022;1253:132267.
4. Hsu C-Y, Rheima AM, Mohammed MS, Kadhim MM, Mohammed SH, Abbas FH, et al. Application of Carbon Nanotubes and Graphene-Based Nanoadsorbents in Water Treatment. BioNanoScience. 2023;13(4):1418-1436.
5. Al-Salman HNK, Falih Ms, Deab HB, Altimari US, Shakier HG, Dawood AH, et al. A study in analytical chemistry of adsorption of heavy metal ions using chitosan/graphene nanocomposites. Case Studies in Chemical and Environmental Engineering. 2023;8:100426.
6. Raya I, Widjaja G, Mahmood ZH, Kadhim AJ, Vladimirovich KO, Mustafa YF, et al. Kinetic, isotherm, and thermodynamic studies on Cr(VI) adsorption using cellulose acetate/graphene oxide composite nanofibers. Appl Phys A. 2022;128(2).
7. Al-Obaidi NS, Sadeq ZE, Mahmoud ZH, Abd AN, Al-Mahdawi AS, Ali FK. Synthesis of Chitosan-TiO_2 Nanocomposite for Efficient Cr(VI) Removal from Contaminated Wastewater Sorption Kinetics, Thermodynamics and Mechanism. Journal of Oleo Science. 2023;72(3):337-346.
8. Asaad Mahdi M, Farhan MA, Mahmoud ZH, Mahdi Rheima A, sabri Abbas Z, Kadhim MM, et al. Direct sunlight photodegradation of congo red in aqueous solution by TiO_2/rGO binary system: Experimental and DFT study. Arabian Journal of Chemistry. 2023;16(8):104992.
9. Mahmoud ZH, Hamrouni A, Kareem AB, Mostafa MA, Jalil alhakim Z, Majeed AH. Synthesis and characterization of chitosan sheet modified by varied weight ratio of anatase (TiO_2) nano mixture with Cr(VI) adsorbing. Kuwait Journal of Science. 2023;50(3):290-299.
10. Mahmoud ZH, Ajaj Y, Hussein AM, Al-Salman HNK, Mustafa MA, Kadhum EH, et al. $CdIn_2Se_4$@chitosan heterojunction

nanocomposite with ultrahigh photocatalytic activity under sunlight driven photodegradation of organic pollutants. Int J Biol Macromol. 2024;267:131465.
11. Velmurugan R, Swaminathan M. A study of mechanism and operational parameters on solar light-induced degradation of Reactive Red 120 dye with AgBr-loaded TiO_2. Res Chem Intermed. 2013;41(2):1227-1241.
12. Farhan MA, Mahmoud ZH, Falih MS. Synthesis and Characterization of TiO_2/Au Nanocomposite Using UV-Irradiation Method and Its Photocatalytic Activity to Degradation of Methylene Blue. Asian J Chem. 2018;30(5):1142-1146.
13. Ismaeel GL, Hussein SA, Daminova G, Sulaiman JMA, Hani MM, Kadhum EH, et al. Fabrication and investigating of a nano-structured electrochemical sensor to measure the amount of atrazine pollution poison in water and wastewater. Chemical Data Collections. 2024;51:101135.
14. AbdulKareem EA, Mahmoud ZH, Khadom AA. Sunlight assisted photocatalytic mineralization of organic pollutants over rGO impregnated TiO_2 nanocomposite: Theoretical and experimental study. Case Studies in Chemical and Environmental Engineering. 2023;8:100446.
15. Putri K, Annisa A, Husain S, Rodiansono R. One-pot Synthesis of Carbon-doped TiO_2 with Bimetallic Ni-Ag co-catalysts in Photodegradation of Methylene Blue under UV and Visible Irradiation. Bulletin of Chemical Reaction Engineering and Catalysis. 2019;15(1):35-42.
16. Mohammadkhani F, Mohammadkhani A, Ajaj Y, Almulla AA, Tameemi ARA, Mahmoud ZH, et al. An experimental study on absorption and catalytic activity of molybdenum-schiff bases complex immobilized on Tl_2O_3–SiO_2 nanoparticles. Case Studies in Chemical and Environmental Engineering. 2024;9:100684.
17. Kapse M, Naik D. From Chitin to Climate-Smart Agriculture: A Bibliometric Analysis of Chitosan Nanoparticle Applications in Crop Stress Mitigation. Journal of Crop Health. 2026;78(2).
18. Verma S, Dutta RK. Adsorptive Removal of Toxic Dyes Using Chitosan and Its Composites. Environmental Chemistry for a Sustainable World: Springer International Publishing; 2019. p. 223-255. http://dx.doi.org/10.1007/978-3-030-17724-9_10
19. Al-Mur BA, Jamal MT. Eco-Friendly Dye Removal Using Chitosan: Characterization and Kinetic Modeling of Methylene Blue and Methyl Orange Adsorption. Polymers. 2026;18(5):546.
20. Suhaimi A, Jawad AH, Kazem HA. Modeling and experimental design optimization of toxic brilliant green dye removal using schiff's base benzaldehyde grafted- modified chitosan: desirability function, reusability, and adsorption mechanism. Colloid Polym Sci. 2025;304(3):629-650.
21. Zawawi NM, Jawad AH, Wilson LD, Alothman ZA, Kazem HA. Biocomposite System of Schiff's Base Grafted Chitosan Biopolymer-Salicylaldehyde Doped with Hydroxyapatite Nano Particles: Characterization, Statistical Optimization and Application for Anionic Dyes Removal. BioNanoScience. 2026;16(2).
22. Ghanbari K, Nejabati F. Ternary nanocomposite-based reduced graphene oxide/chitosan/Cr_2O_3 for the simultaneous determination of dopamine, uric acid, xanthine, and hypoxanthine in fish meat. Analytical Methods. 2020;12(12):1650-1661.
23. Cao S, Guo J, Ma J, Chen E, Pang J, Zhang S, et al. Effective removal of hexavalent chromium with magnetically reduced graphene oxide bentonite. Clay Minerals. 2023;58(1):7-18.
24. Solmaz A, Ilter Z, Kaya I. Synthesis, Characterization, Thermal Behavior, and Dielectric Properties of Methacrylate Polymers Containing Imine Bonding. J Electron Mater. 2021;50(9):5348-5358.
25. Ghotekar S, Pansambal S, Bilal M, Pingale SS, Oza R. Environmentally friendly synthesis of Cr2O3 nanoparticles: Characterization, applications and future perspective – a review. Case Studies in Chemical and Environmental Engineering. 2021;3:100089.
26. Haque J, Srivastava V, Chauhan DS, Lgaz H, Quraishi MA. Microwave-Induced Synthesis of Chitosan Schiff Bases and Their Application as Novel and Green Corrosion Inhibitors: Experimental and Theoretical Approach. ACS Omega. 2018;3(5):5654-5668.
27. Güngör Ö, Gürkan P. Synthesis and characterization of higher amino acid Schiff bases, as monosodium salts and neutral forms. Investigation of the intramolecular hydrogen bonding in all Schiff bases, antibacterial and antifungal activities of neutral forms. J Mol Struct. 2014;1074:62-70.
28. Cheah S-Y, Phang Y-K, Koh M-X, Chia-Yen Lim S, Djearamane S, Subramaniam H, et al. Eco-sustainable synthesis of chromium oxide (Cr_2O_3) nanoparticles via pomegranate husk extract: calcination-driven control of structure and properties. Green Processing and Synthesis. 2025;15(1).
29. A. Shukur D, Aziz BK, Aziz SB. FTIR, XRD, electrical and dielectric characteristics of solid polymer blend electrolytes based on chitosan: dextran inserted with $NH_4CF_3SO_3$ salt as proton provider. Int J Polym Anal Charact. 2026;31(6):737-763.
30. Sharma P, Thakur D, Kumar D. Novel Enzymatic Biosensor Utilizing a MoS_2 /MoO_3 Nanohybrid for the Electrochemical Detection of Xanthine in Fish Meat. ACS Omega. 2023;8(35):31962-31971.
31. Chitosan-Coated Superparamagnetic Fe3O4 Nanoparticles for Magnetic Resonance Imaging, Magnetic Hyperthermia and Drug Delivery. American Chemical Society (ACS).
32. Albqmi M, Alali I, Alhathlaul N, Alsobai NA, Hasan I, Yadav AK, et al. Engineering a durable hybrid supercapacitor via synergistic rose-like bimetallic MnCoTe embedded in rGO matrix. Diamond Relat Mater. 2026;165:113664.
33. AbdelAll N, Mimouni A, Rayan AM, Khouqeer GA, Hassan MA, Ahmed MR. Sol–gel synthesis and comprehensive characterization of MgO nanostructures: structural, optical, and dielectric insights. Sci Rep. 2026;16(1).
34. Albqmi M, Algethami N, Daoud E, Sasikumar Y, Sharma R, Ali W, et al. In-situ synthesized IRMOF-1/graphene oxide-carbon nanotubes hybrid for boosting electrochemical hydrogen storage. J Alloys Compd. 2026;1059:187157.
35. Ahmed HM, Joer AAA, Hussein UA-R, Al-Anbari HHA, Abdulwahid AS, Salah G, et al. Gold Nanoparticles in Biomolecular Interactions for Biomedical Applications. BioNanoScience. 2026;16(3).
36. Rashid AK, Ahmed HM, Mageed ZN, Mahmoud ZH, Mhaibes RM. Preparation and antimicrobial activity of Mono-, Bis, and Tris-4,9-Dihydroxy-7,7-Dimethyl-5-(mono-substituted-aryl)-Hexahydro-Indeno[1,2-b]Indole-9,10-Dione derivatives. Med Chem Res. 2026;35(3):594-624.
37. Alali I, Khan RA, Albqmi M, Koo BH, Ali W, Alsobai NA, et al. Novel magnetic gellan gum hydrogel nanocomposite with polydopamine and functionalized halloysite nanotubes for efficient butylparaben adsorption from wastewater. Int J

Biol Macromol. 2026;338:149689.
38. Visible Light Photocatalytic Degradation of Methylene Blue Dye and Pharmaceutical Wastes over Ternary NiO/Ag/TiO_2 Heterojunction. American Chemical Society (ACS). http://dx.doi.org/10.1021/acsomega.3c01766.s001
39. Majeed AH, Hussen WA, Abd AN, Mahmoud ZH, kianfar E. Graphene–tungsten oxide hybrid nanocomposites for high-performance dielectric films in conductive polymer matrices. South African Journal of Chemical Engineering. 2025;53:303-318.
40. Mhaibes RM, Kadhum AAH, Al-Salman HNK, Mahmoud ZH, Mudhafar M, Lahhob QR, et al. Recent update on catalytic activity of N-heterocyclic carbene supported on graphene nanosheets: A mini review. J Organomet Chem. 2025;1034:123660.
41. Mahmoud ZH, Al-Salman HNK, Hussein UA-R, Hameed SM, Hussein AA, Abbas JM, et al. Recent Advances in the Applications of Smart Nanomaterials in Biomedicine: A Review. Nano LIFE. 2025;16(03).
42. Li C, Nie Y, Yang T, Chen B, Tong L, Yuan Y, et al. Thermal effects in breakthrough curves of hydrogen purification using analytically derived isosteric heat of adsorption from Langmuir-Freundlich model. Int J Hydrogen Energy. 2026;261:156642.
43. Christensen JM. The theoretical basis for the Freundlich adsorption isotherm. Surface Science. 2026;774:123025.
44. Tlili A, Dridi I, Mlaiki F, Jedidi N, Antisari LV, De Feudis M. Freundlich, Langmuir and Temkin Isotherms for Assessing Boron Adsorption-Desorption in Different Soil Types in Tunisia. Eurasian Soil Science. 2026;59(4).
45. Mahanty B, Behera SK, Sahoo NK. Misinterpretation of Dubinin–Radushkevich isotherm and its implications on adsorption parameter estimates. Sep Sci Technol. 2023;58(7):1275-1282.